Neural Networks for Inverse Kinematics Problems in Robotics

Franziska Schwaiger
Matriculation number: 03658670

Thomas Barthel Brunner
Matriculation number: 03675118

Introduction

In our project, we are evaluating the feasibility of using neural networks for inverse kinematics problems in robotics. In this report, we outline the progress made and discuss the results we have obtained.

Methods

Robot Simulations

To train and test our models, we developed simulations of planar robotic arms with revolute joints. As we are interested in testing the limits of our models, we created simulations of arbitraty degrees of freedom (DOFs). In general, the forward kinematics equations of a planar robot arm with link lengths l_i and N revolute joints with joint angles θ_i can be described as:

$$x_{TCP} = \sum_{i=1}^{N} l_i \cos\left(\sum_{j=1}^{i} \theta_j\right) \tag{1}$$

$$y_{TCP} = \sum_{i=1}^{N} l_i \sin\left(\sum_{j=1}^{i} \theta_j\right) \tag{2}$$

$$\theta_{TCP} = \sum_{i=1}^{N} \theta_i \tag{3}$$

These equations were modified for fast vectorized numerical computation by the element-wise computation of the sine and cosine of the matrix multiplication of the joint angles vector $\boldsymbol{\theta} = [\theta_1, \theta_2, ...]^{\mathrm{T}}$ with an upper triangular matrix with ones as elements $\boldsymbol{U}$. The results are then multiplied with the link lengths vector $\boldsymbol{l} = [l_1, l_2, ...]^{\mathrm{T}}$, as shown in Equations 4 and 5.

$$x_{TCP} = \cos\left(\boldsymbol{\theta}\ \boldsymbol{U}\right)\boldsymbol{l} \tag{4}$$

$$y_{TCP} = \sin\left(\boldsymbol{\theta}\ \boldsymbol{U}\right)\boldsymbol{l} \tag{5}$$

In our current setup, we do not take the angle of the tool center point (TCP) into consideration. Thus, the location of the TCP is defined by its x, y coordinates. As a result of this, all simulations with more than 2 DOF can up to infinite solutions of the inverse kinematics for a given TCP position. The 2 DOF robot arm can have up to two solutions.

Dataset

The dataset used for training is composed of one million samples of robot configurations for each DOF. Figure **??** shows an illustration of the datasets. Each configuration was sampled from a normal distribution $\theta_i \sim \mathcal{N}(\mu = 0, \sigma = 0.2)$. Thus, the dataset is composed mostly of configurations in which the robot arm is extended. This reflects real-world use cases of robot arms, which have limited workspaces and whose tasks are focused on one section of the workspace. Moreover, limiting the range of the joints improved the performance of the networks, as this avoids the discontinuity in the angles at $\theta = \pi$.

Considering Singularities

As already mentioned in the previous section, we avoid discontinuities by restricting the configuratoin space of the robot. Yet we implemented two approaches which consider this discontinuity in the angles at $\theta = \pi$ to generalize the implemented networks to inverse kinematics problems.

First approach: The first approach uses a non-minimal parameterization of ...

Second approach:

Network Architectures

As described in the midterm report, we implemented two network architecture for generating the full posterior of the joint angles: Unlike VAE, cVAE are able to control the data generation process by conditioning the latent space z. Considering the application of inverse kinematics, samples are drawn from $p(z) \sim N(0, 1)$ and the predicted posterior of the joint angles is then generated conditioned on the end-effector position.

INNs model a bijective mapping from the joint angles to the end-effector position by stacking invertible blocks together. Here, the dimensionality of the joint angles x is the same as the concatenated output consisting of the latent space z and the end-effector position y. The predicted posterior of the joint angles is then generated similar to cVAE by sampling from $p(z) \sim N(0, 1)$ and then running the network backwards condition on y.

Additionally, INNs share properties with normalizing flows [1], [2] which gradually transform a normal density into the desired datadensity. They are also bijective and for both normalizing flows and INNs, a tractable Jacobian exists hich allows explicit computation of posterior probabilities.

As stated in [3], the INN only needs to be trained on the well-understood forward process and then the inverse process can be obtained for free by just running the network backwards at prediction time. The also mention that results can be improved with additional unsupervised backward training. When applying INNs to the inverse kinemtaics proble, we found that to match the performance of the cVAE, unsupervides brackward training is crucial. This results in two network passes per training step to accumulate the gradients and slows down training a lot. Additionally, when training INNs the parameters need to be adjusted carefully as training can be become unstable.

Hyperparameter Optimization

For our tests, we trained a network for each robot simulation (DOF). Thus, the sizes and selection of hyperparameters of each network had to match the compleity of the simulation. To compare the performance of the networks across different DOFs in a fair setting, we used Tune [4] to perform a random search of the hyperparameters. To reduce computation time, we trained the models using a subset of the main dataset, which was composed of $1e4$ samples.

Implementation

The previous two model architectures (cVAE and INN) have been implemented in PyTorch and are inspired by existing implementations in [5], [6]. We utilized the Google Compute Engine to train our models.

Experimental Evaluation

Evaluation protocol

We extended the DoF of the robots up to 15 DoF and performed Baysian optimization for the hyperparameters for $DoF = [4, 6, 10, 15]$ by evaluating 100 points in the hyperparameters space for each DoF. But now it is important to mention that due to HPO, the number of trainable parameters differs between cVAE and INN. The batch size is was kept fixed to 1000 for both networks. For the cVAE, we optimized the learning rate, the weight decay, the number of hidden layers for the encoder and decoder and the amount of neurons per layer. For the INN, we optimized the learning rate, the weight decay, the number of coupling layers, the amount of layers per subnet and also the number of neurons per subnet layer. Both networks have been trained for 60 epochs on a dataset with 1 million samples and a train and test spit of 70 and 30, respectively. For evaluation, we used again the two evaluation metrics we have already described in the midterm report:

1. The average mismatch between the true posterior obtained via rejection sampling and the predicted posterior computed for now 1000 instead of 100 randomly but fixed chosed samples from the test dataset.

2. The average re-simulation error computed on the whole test dataset by applying the simulation for the true forward kinematics to the generated joint angles and measure the mean squared distance between the ground truth end-effector position and the re-simulated end-effector position resulting from the predicted joint angles.

Results

The hyperparameters for the cVAE and INN chosen by Bayesian optimization are depicted in Table I and II, respectively. Because of HPO, the number of parameters per robot is not approximately equal, anymore. As it can be seen in the tables, the best architectures are not the architectures with the most numbers of trainable parameters. This also shows that the hyperparameters search space is sufficient.

For both networks, the mismatch of the posterior and the re-simulation error is plotted over the number of parameters in Fig. and 2, respectively. Each plotted point is labelled with the corresponding robot of different DoF. As it can be seen, when increasing the number of degrees of freedom, the number of parameters does not have to be increased, as well. This is also a result of the HPO. The mismatch of the predicted posterior (see Fig.) with the ground truth posterior obtained from rejection sampling is less for the INN as for the cVAE. But in contrast to that, the cVAE performs consistently better on the re-simulation error as the INN (see Fig. 2).

Look at the convex hull!!!!!

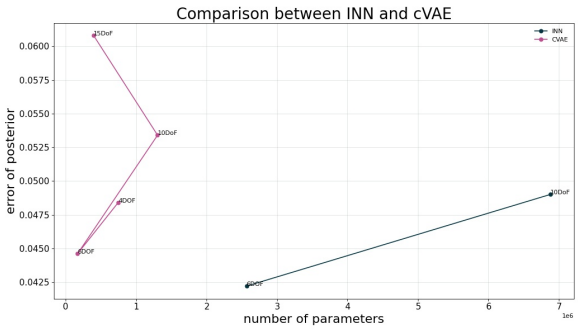

Fig. 1. Results. Mismatch of posterior. Needs to be completed.

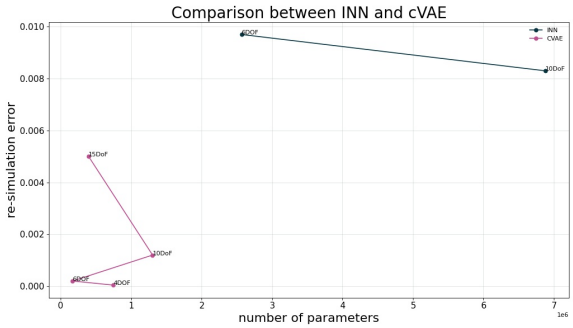

Fig. 2. Results. Mismatch of re-simulation error. Needs to be completed.

DOF	learning rate	weight decay	# hidden layers	# neurons	# trainable parameters
6	...	...	...	...	...
10	...	...	...	...	...
15	...	...	...	...	...

TABLE I
HYPERPARAMETERS FOR CVAE WHICH HAS BEEN TRAINED ON A PLANAR ROBOT WITH N DOF WITH $N = [4, 6, 10, 15]$.

DOF	learning rate	weight decay	# coupling layers	# subnet layers	# neurons per subnet layer	# trainable parameters
6	...	...	...	...	...	...
10	...	...	...	...	...	...
15	...	...	...	...	...	...

TABLE II
HYPERPARAMETERS FOR INN WHICH HAS BEEN TRAINED ON A PLANAR ROBOT WITH N DOF WITH $N = [4, 6, 10, 15]$.

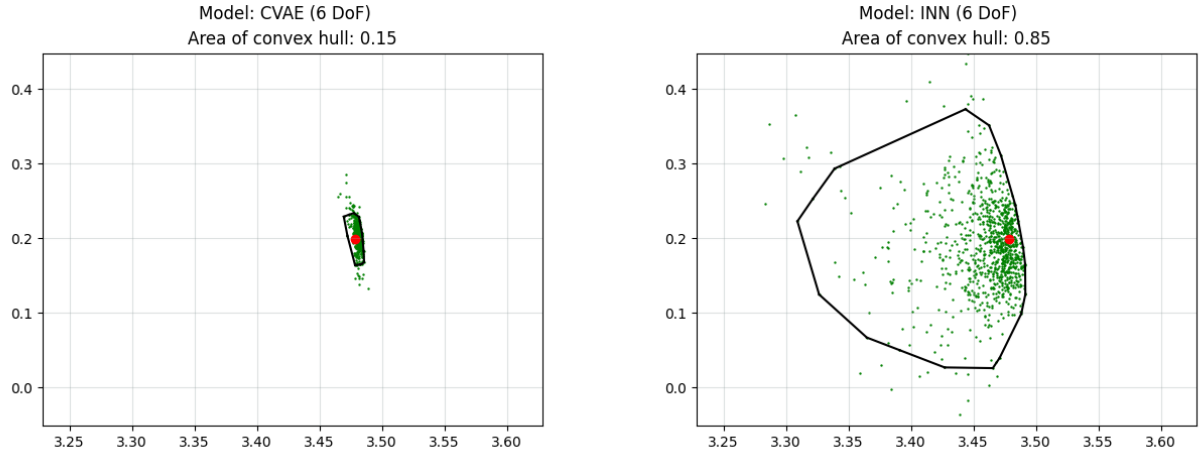

(a) cVAE (b) INN

Fig. 3. Area of the convex hull of the 0.97 percentile of the re-simulated end-effector coordinates with the ground truth end-effector position at $(x, y) = [3.47, 0.19]$ and 1000 samples. Number of DoF: 6.

CONCLUSION

We have compared the two networks cVAE and INN to the application of inverse kinematics. ... The focus in this work was on the study of the INN which in theory, is a powerful tool to recover the full posterior parameters distribution. When applied to inverse kinemtaics though, ...

REFERENCES

[1] E. G. Tabak and E. Vanden-Eijnden, "Density estimation by dual ascent of the log-likelihood," *Communications in Mathematical Sciences*, vol. 8, no. 1, pp. 217 – 233, 2010. [Online]. Available: https://doi.org/

[2] E. Tabak and C. Turner, "A family of nonparametric density estimation algorithms," *Communications on Pure and Applied Mathematics*, vol. 66, no. 2, pp. 145–164, Feb. 2013, copyright: Copyright 2012 Elsevier B.V., All rights reserved.

[3] L. Ardizzone, J. Kruse, S. J. Wirkert, D. Rahner, E. W. Pellegrini, R. S. Klessen, L. Maier-Hein, C. Rother, and U. Köthe, "Analyzing inverse problems with invertible neural networks," *CoRR*, vol. abs/1808.04730, 2018. [Online]. Available: http://arxiv.org/abs/1808.04730

[4] R. Liaw, E. Liang, R. Nishihara, P. Moritz, J. E. Gonzalez, and I. Stoica, "Tune: A research platform for distributed model selection and training," *arXiv preprint arXiv:1807.05118*, 2018.

[5] graviraja, "pytorch-sample-codes," https://github.com/graviraja/pytorch-sample-codes, 2019.

[6] "Freia," https://github.com/VLL-HD/FrEIA/blob/master/FrEIA/, 2020.

[7] K. Sohn, H. Lee, and X. Yan, "Learning structured output representation using deep conditional generative models," in *Advances in Neural Information Processing Systems*, C. Cortes, N. Lawrence, D. Lee, M. Sugiyama, and R. Garnett, Eds., vol. 28. Curran Associates, Inc., 2015, pp. 3483–3491.

[8] M. Mirza and S. Osindero, "Conditional generative adversarial nets," *CoRR*, vol. abs/1411.1784, 2014. [Online]. Available: http://arxiv.org/abs/1411.1784

[9] A. Gretton, K. M. Borgwardt, M. J. Rasch, B. Schölkopf, and A. J. Smola, "A kernel method for the two-sample problem," *CoRR*, vol. abs/0805.2368, 2008. [Online]. Available: http://arxiv.org/abs/0805.2368

[10] Y. Zhou, C. Barnes, L. Jingwan, Y. Jimei, and L. Hao, "On the continuity of rotation representations in neural networks," in *The IEEE Conference on Computer Vision and Pattern Recognition (CVPR)*, June 2019.

[11] J. Kruse, L. Ardizzone, C. Rother, and U. Köthe, "Benchmarking invertible architectures on inverse problems," Tech. Rep. i, 2019.

[12] B. Choi and C. Lawrence, "Inverse kinematics problem in robotics using neural networks," Tech. Rep., 1992.

[13] L. Dinh, J. Sohl-Dickstein, and S. Bengio, "Density estimation using real NVP," *CoRR*, vol. abs/1605.08803, 2016. [Online]. Available: http://arxiv.org/abs/1605.08803

[14] D. P. Kingma and M. Welling, "Auto-encoding variational bayes," 2014.

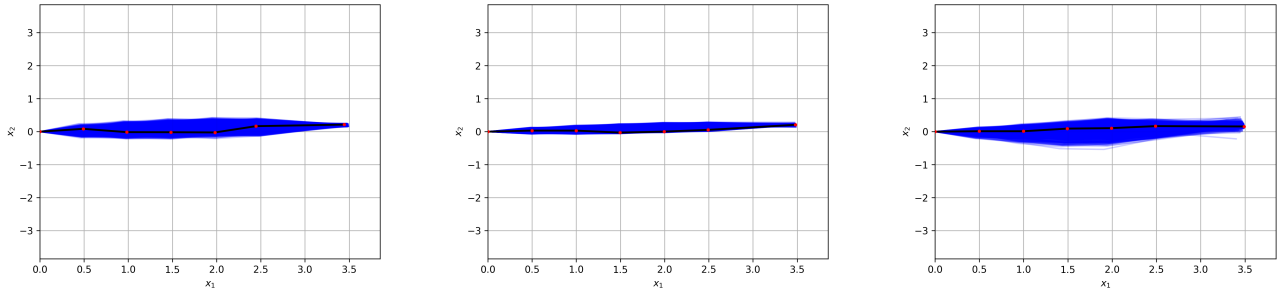

(a) Rejection Sampling (b) cVAE (c) INN

Fig. 4. Arm configuration of a planar manipulator with 6 revolute joints and end-effector position at $(x, y) = [3.47, 0.19]$. 100 samples are drawn from each model's predicted posterior $\tilde{p}(x|y_{gt})$, one random sample configuration is highlighted. $e_{posterior} = 0.032$ for the cVAE and $e_{posterior} = 0.018$ for the INN.